Do High Order Accurate Schemes for the Convection Terms always Guarantee the Improved Prediction for Nuclear Safety Problems?

Gong Hee Lee [a]*, Ae Ju Cheong [b]
[a]*Korea Institute of Nuclear Safety, Daejon, 305-338*
[b]*Nuclear Safety Research Department, Korea Institute of Nuclear Safety, Daejon, 305-338*
[*]*Corresponding author: ghlee@kins.re.kr*

1. Introduction

Spatial discretization errors result from both the numerical order of accuracy of the discretization scheme, and from grid spacing. It is well known that second, or higher, order discretization schemes are potentially able to produce high-quality solutions. In addition, when either the flow is not aligned with the grid, or is complex, it is recommended that the first order discretization scheme not be used for the convection term, if possible [1]. However, the higher-order scheme can also result in convergence difficulties and instabilities at certain flow conditions.

In this study, to examine the effect of the numerical order of accuracy of the discretization scheme on the prediction accuracy for the nuclear safety problems, simulations were conducted with the commercial CFD (Computational Fluid Dynamics) software, ANSYS CFX R.14 and FLUENT R.14. The predicted results were compared with the measured data.

Three test cases were selected; (1) moderator test vessel (Stern Laboratories Inc.), (2) 1/5 scaled-down APR+ (Advanced Power Reactor Plus) model (KAERI), (3) MATiS-H (Measurement and Analysis of Turbulent Mixing in Subchannles-Horizontal) facility (KAERI).

2. Moderator Test Vessel (Stern Lab. Inc.)

2.1 Overview of Test Facility

A schematic diagram of test facility was shown in Fig. 1. The vessel had a transparent polycarbonate cylindrical shell with a diameter of 2m and a length of 0.2m. By restricting the axial dimension of the vessel, a predominantly 2-dimensional flow could be obtained. A total of 440 electrical tube heaters (0.033m in diameter and 0.2m in length) were installed on a 0.071m square pitch pattern. Light water entered the vessel through two symmetrically placed inlet nozzles, which shot vertically directed jet-type flow at the horizontal centerline. One outlet nozzle whose length was same as that of a tube heater was installed at the bottom of the vessel. Fluid velocity and temperature were measured with a laser Doppler anemometer (LDA) and thermocouples. More detailed descriptions of test facility can be found in Reference [2].

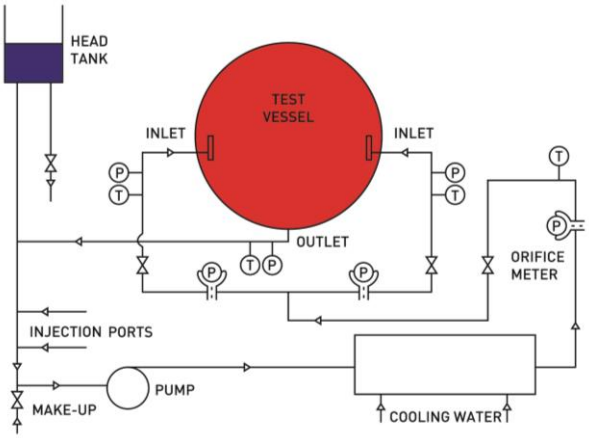

Fig. 1. Schematic diagram of test facility.

2.2 Test Conditions

The test matrix consisted of four test conditions as shown in Table I. In this study, CFD simulation was conducted under both isothermal and nominal condition. Test parameters such as a total inlet flow rate, total heat load, and an outlet temperature were determined by a similarity analysis of momentum and energy equations, and therefore their magnitudes were closely related with the operating conditions of a typical CANDU reactor at full power.

Table I: Test Matrix

Test conditions	Inlet flow rate (kg/s)	Heat load (kW)
Isothermal	**2.4**	**0**
Nominal	**2.4**	**100**
Low flow	2.0	100
Symmetry*	2.4	100

* Insertion of a dividing wall along the vertical centreline of test vessel

2.3 Geometry Modeling

Although the porosity of a CANDU reactor is high (about 0.83) enough to allow the porous medium assumption to be used, this assumption has several possible weaknesses. In this study, as shown in Fig. 2, the real geometries of 440 electrical tube heaters were considered, and no porous medium assumption was used.

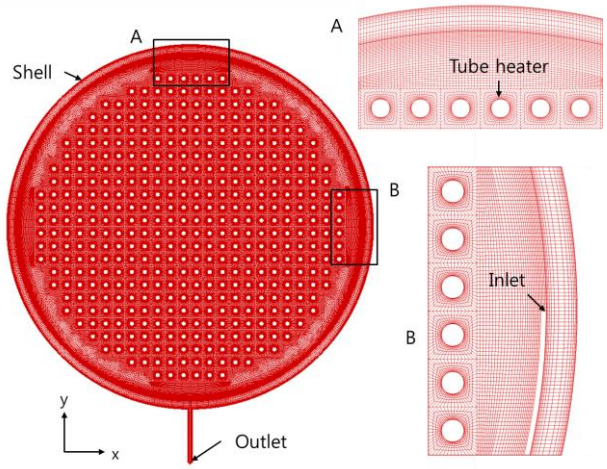

Fig. 2. Grid system.

2.4 Numerical Modeling

The flow inside the calandria vessel was assumed to be steady, incompressible and turbulent. The pressure-velocity coupling was handled by the SIMPLE algorithm. The solution was considered to be converged when the residuals of variables were below 10^{-5} (10^{-7} for energy equation) and the variations of the target variables were small.

In case of nominal condition, the effect of buoyancy force was modeled with the Boussinesq approximation. A constant volumetric expansion coefficient of 4.6×10^{-4} was used. The generation of turbulent kinetic energy due to buoyancy was considered in k and ε equation. Simulation was conducted with the commercial CFD software, FLUENT R.14.

In a previous study [3], turbulence models available in FLUENT R.14, for example k-ε model and Reynolds Stress model (RSM), were used to simulate the turbulent flow inside the calandria vessel. Although RSM may have the possibility of giving the superior performance to the k-ε model, especially for flow with strong swirl and rotation, this model demands a significant increase in computing time, and has often the convergence problem. On the other hand, the k-ε model showed the best agreement with the experimental data. More detailed descriptions of the k-ε model can be found in the ANSYS FLUENT user's guide [4].

As shown in Fig. 2, the hexahedral grid system was generated for the computational domain that had the same dimension as the test vessel. Total numbers of elements were 3.3×10^{6}. Maximum value of y^{+} at the downcomer was 117 for isothermal condition and 152 for nominal condition. Minimum orthogonal quality was 0.507 and maximum skewness was 0.49.

Constant flow rate of total 2.4kg/s (nozzle width of 8mm) was imposed at normal to inlet boundary. Inlet fluid temperature was 55.5℃. Turbulence intensity at inlet was assumed to be 5.0%. Average pressure over whole outlet option with the relative pressure of 0 Pa was used as an outlet boundary condition. No-slip condition was applied on the solid wall. Uniform heat flux (W/m^2) which corresponded to 100kW DC (Direct Current) power, was imposed on the heater wall and adiabatic condition on the other walls. In order to model the near-wall region, wall function approach was used.

2.5 Results and Discussion

2.5.1. Isothermal condition. Fig. 3 shows the vertical (y-direction) velocity profile along the vertical centerline (x=0). The 1st order accurate upwind differencing (1st-1st) for the convection-terms-of-momentum equations and turbulence equations under-predicted the magnitude of the vertical velocity in most regions; compared with the 2nd order accurate upwind differencing (2nd-2nd). One of reason may be that the use of the low-order accurate discretization scheme causes the numerical diffusion and consequently affects the magnitude of the vertical velocity.

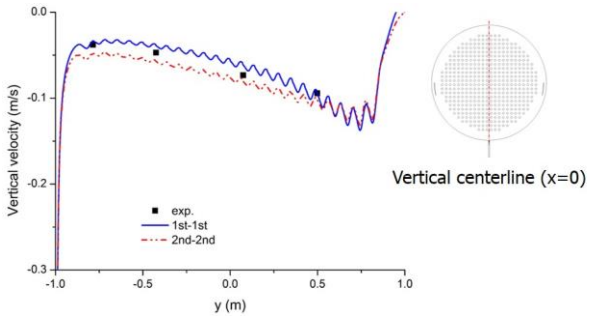

Fig. 3. Vertical velocity profile along the vertical centerline (x=0).

Fig. 4 shows the tangential velocity profile near the circumferential wall along the radial line which was located at 30 degree counter-clockwise rotation from horizontal centerline. The predicted velocity profiles was nearly same regardless of the order of accuracy for the discretization scheme.

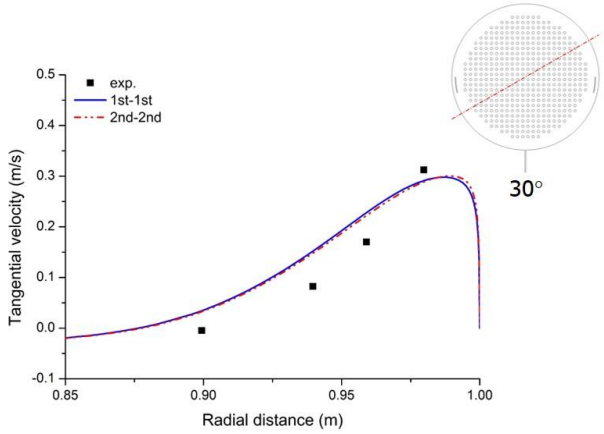

Fig. 4. Tangential velocity profile along the radial line.

2.5.2. Nominal condition. In the CANDU reactor, moderator subcooling is the difference between the heavy water saturation temperature and the local fluid

temperature at any specific location. Therefore under-prediction of the local fluid temperature is non-conservative in the regulatory perspective.

Fig. 5 shows the temperature profile at the vertical centerline (x=0). The prediction with the 1st order accurate upwind differencing (1st-1st) showed the better agreement with measurement. The 2nd order accurate upwind differencing (2nd-2nd) under-predicted local fluid temperature especially in the range of -0.45m<y<0.72m; compared with the 1st order accurate upwind differencing (1st-1st).

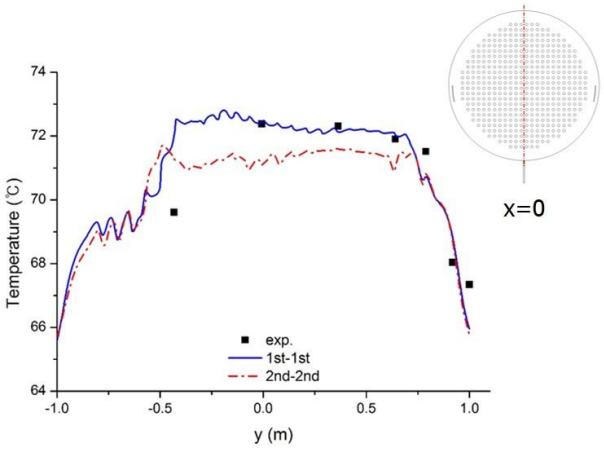

Fig. 5. Temperature profile along vertical centerline (x=0).

3. ACOP (KAERI)

3.1 Overview of Test Facility

APR+ Core Flow & Pressure Test Facility (ACOP), installed in the KAERI, is a 1/5 scaled-down model of APR+. It consists of a reactor vessel with two coolant loops (i.e., four cold legs and two hot legs). The internal structures of the reactor model (e.g., flow skirt and upper/lower core structures), had almost the same shapes as those in the original APR+ and satisfied geometrical similarity [5]. A total of 257 core simulators were installed in the reactor model. The core-inlet flow-rate distribution could be obtained by measuring the differential pressure and discharge coefficients at the venturi region of the each core simulator [5]. The upper head of the reactor, and some core-bypass flow-paths were neglected in the reactor model because these parts were expected to have little influence on the core-inlet flow-rate distribution.

3.2 Test Conditions

The test matrix consists of three flow conditions, i.e., the symmetric or asymmetric flow conditions for 4-pumps operation, and the flow condition for 3-pumps operation. In this study, CFD simulation was conducted under the symmetric flow condition for 4-pumps operation. Under this condition, the Reynolds number was about 8.6×10^5 in the downcomer.

3.3 Geometry Modeling

APR+ reactor internals are complex structures which support fuel assemblies, control rods and measuring instruments. The internal structures, especially those located in the upstream of the reactor core, may have a significant influence on the core-inlet flow-rate distribution; depending on both their shapes, and the relative distance between the internal structures and the core inlet [6]. Therefore an exact representation of these internal structures is needed for CFD simulation of the core-inlet flow-rate distribution. However, such an approach requires a great deal of computing resources to analyze the real-flow phenomena inside a reactor.

In this study, as shown in Fig. 6(a), among the reactor internal structures located upstream of reactor core, the real geometries of a flow skirt, lower-support-structure-bottom plate and ICI (In-Core Instrumentation) nozzle support plate, were considered because these internal structures could significantly influence the flow-rate distribution at the core inlet.

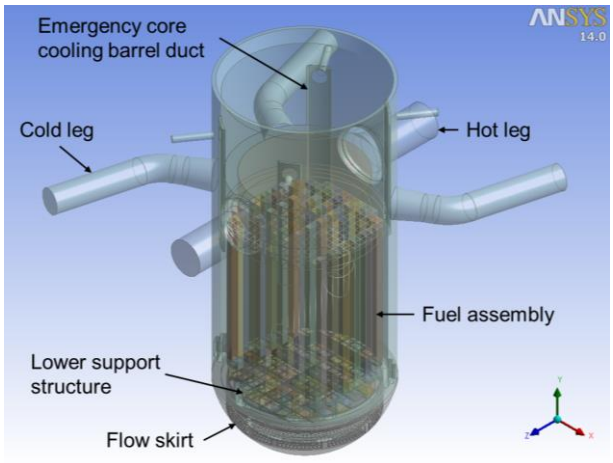

(a) Full geometry

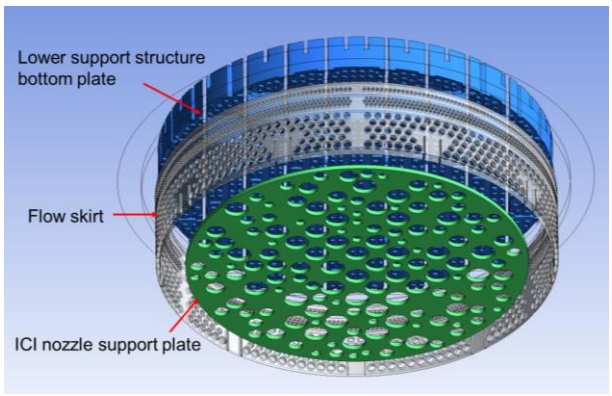

(b) Details of lower support structure

Fig. 6. The computational domain.

Meanwhile, to reduce total numbers of elements and thus minimize the required amount of computation, fuel assemblies and some internal structures (e.g., control-

element guide tubes) were simply considered as each bulk volume (porous domain). Then, in order to reflect the velocity field and pressure drop occurring in the real-flow region; porosity and Isotropic Loss Models [7] were applied to the porous domain.

Porosity is the ratio of the volume of fluid region to total volume; including both fluid and solid regions. It has an effect on flow acceleration in the porous domain. In this study, the porosity was determined by considering the real geometry of the reactor internal structures. A momentum source was used to model the momentum loss in the porous domain; which corresponds to a pressure drop in real reactor vessel. Loss coefficients were adjusted to match the magnitude of the pressure drop found in the porous domain, with those of the measurement.

3.4 Numerical Modeling

The flow inside the scaled-down APR+ model was assumed to be steady, incompressible, isothermal and turbulent. The solution was considered 'converged' when the residuals of the variables were below 6×10^{-4}, and the variations of the target variables were small. Simulation was conducted with the commercial CFD software, ANSYS CFX R.14.

The k-ε model, which is one of the most prominent Reynolds Averaged Navier-Stokes (RANS)-based turbulence models, was used to simulate the turbulent flow inside the scaled-down APR+. The reason is that this model has proven to be numerically stable and has offered a good compromise in terms of accuracy and robustness. In a previous study [8], turbulence models available in ANSYS CFX R.13, for example k-ε model, Shear Stress Transport (SST) model, and SSG (Speziale, Sarkar and Gatski) Reynolds Stress model, were used to examine the turbulent flow inside the scaled-down APR+. Although the reactor internal-flow pattern differed locally; depending on the turbulence models used, the k-ε model showed the best agreement with the experimental data. More detailed descriptions of the k-ε model can be found in the ANSYS CFX-solver modeling guide [7].

A hybrid mesh, made up of tetrahedrons, pyramids and prisms, was generated to prevent the oversimplification of the geometry, and to have more efficient mesh distribution. Prism layers were used to get higher resolution in the near-wall region. Total numbers of elements were 7.3×10^{7}. Maximum value of y+ at the downcomer was 305.

By referring to the test condition [5]; an inlet flow-rate of 135 kg/s was imposed at each cold leg. Turbulence intensity at the inlet was assumed to be 5 %. Light water at 60℃ was used as the working fluid. The 'average pressure over the whole outlet' option; with a relative pressure of 0 Pa, was used at each hot leg as an outlet-boundary condition. A no-slip condition was applied at the solid wall. To model the flow in the near-wall region, scalable wall functions were applied.

3.5 Results and Discussion

Fig. 7 shows distribution of the normalized core-inlet mass-flow rate along the core centerline (A-A'). With the aid of a flow skirt, a lower-support-structure-bottom plate controls the mass-flow rate distribution at core inlet. In the experiment [9], a relatively high inlet-mass flow-rate was found in the core outer boundary because the size of the flow holes in the lower-support-structure-bottom plate increased in this region.

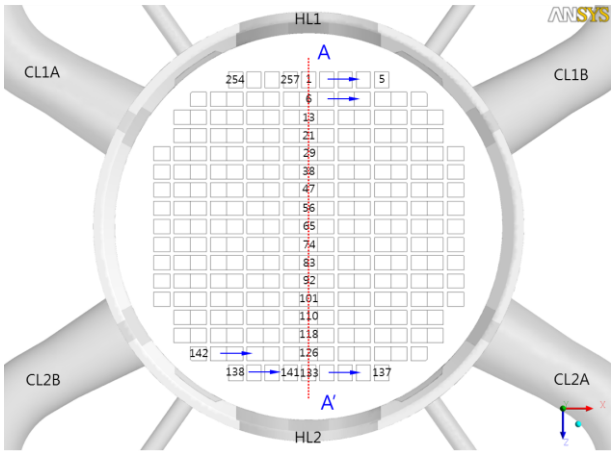

(a) Numbering of fuel assemblies

(b) Normalized core inlet mass flow rate

Fig. 7. Distribution of the normalized core inlet mass flow rate along core centerline (A-A′).

As shown in Fig. 7(b), while all combination types of the discretization scheme for the convection term predicted the similar flow pattern, 1st order accurate upwind differencing (up-up) showed the best agreement with the measured data (see Table II).

Table II: The average difference between calculated and measured distribution of the normalized core-inlet mass-flow rate along the core centerline (A-A')

	up-up	hi-hi
Difference (%)	6.77	8.49

Table III shows the minimum and maximum magnitudes of the normalized, core inlet mass-flow rate at the core-inlet plane. The magnitude is the ratio of the mass-flow rate per each fuel assembly, to the average mass-flow rate at the core-inlet plane.

High resolution scheme (hi-hi) a little bit under-predicted the minimum and maximum magnitudes of the normalized, mass-flow rate at the core-inlet plane; compared with the 1st order accurate upwind differencing (up-up).

Table III: The minimum and maximum magnitudes of the normalized, mass-flow rate at the core-inlet plane.

	Exp.		up-up		hi-hi	
Normalized mass flow rates (%)	Min.	Max.	Min.	Max.	Min.	Max.
	86	126	82	144	80	143

4. MATiS-H (KAERI)

4.1 Overview of Test Facility

MATiS-H test facility, installed in the KAERI, was used to perform hydraulic tests in a rod bundle array under the unheated conditions. As shown in Fig. 8, test rig consists mainly of a water storage tank, a circulation pump, and a test section.

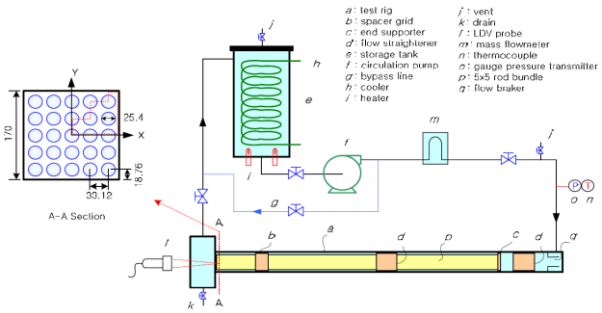

Fig. 8. Schematic diagram of test facility.[10]

The main body of the horizontal test section comprises a 4.67 m-long square duct of inner dimensions 0.17×0.17 m, containing a 3.863m-long 5×5 rod bundle array. Outer diameter of a fuel rod, rod-to-rod pitch, and rod-to-wall pitch were 25.4 mm, 33.12 mm, and 18.75mm, respectively. The hydraulic diameter (D_h) of the flow cross-section was 24.27 mm.

"Split-type" spacer grid, which featured two vanes being bent through an angle of 30° with respect to the horizontal, was installed in the rod bundle for enhancing the lateral turbulent mixing in the subchannels..

Detailed measurements of velocity components in subchannels have been obtained using a two-component LDA system at four different axial locations (Z = 0.5, 1.0, 4.0 and 10D_h) from the downstream edge of the mixing vane tip. Turbulence intensities and vortices in the subchannels were then evaluated from the measured velocity components.

The combined uncertainties of the LDA velocity measurements for all lateral and axial components, normalized with respect to the axial bulk velocity, were estimated to be 4.8%~ 5.1% with 95% confidence.

4.2 Test Conditions

Light water at 35℃ and 156.9kPa was used as the working fluid. The mass flow rate was 24.2kg/s resulting in a bulk velocity of 1.5m/s. The Reynolds number based on the hydraulic diameter (D_h) was 50,250. The mean values and their uncertainties of test conditions are summarized in Table IV.

Table IV: Test Conditions.[10]

Parameters	Unit	Mean value	Uncertainty (%)
Mass flow rate	kg/s	24.2	0.29
Temperature	℃	35	2.90
Pressure	kPa	156.9	0.39
Bulk velocity	m/s	1.5	0.37
Reynolds number		50,250	2.01

4.3 Geometry Modeling

The original CAD file of the "split-type" spacer grids, provided by MATiS-H benchmark organizers, was used for the mesh generation. As shown in Fig. 9, only small gaps between rods and the so-called buttons (i.e. small cylinders used for spacer and rod fixation) were filled by projecting the buttons as solid cylinders flush with the rods because these gaps would not influence the flow distributions due to their small size and would require significantly higher effort to generate the fine mesh.

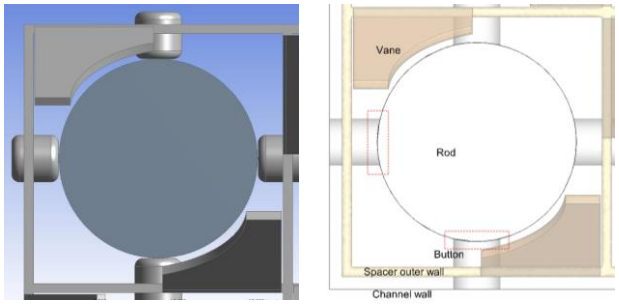

(a) Before change (b) After change

Fig. 9. Geometry simplification.

4.4 Numerical Modeling

The flow inside the fuel assembly was assumed to be unsteady, incompressible, isothermal and turbulent. The 2nd Order Backward Euler scheme was used for the transient term. A time step of 0.001sec was used with

the maximum 10 iterations per time step. Total simulation time was 2sec.

The solution was considered 'converged' when the residuals of the variables were below 10^{-5} at each time step. Simulation was conducted with the commercial CFD software, ANSYS CFX R.14.

The SAS (Scale-Adaptive Simulation)-SST model was used to simulate the turbulent flow inside the fuel assembly. The information provided by the von Karman length-scale allows SAS models to dynamically adjust to resolved structures in URANS (Unsteady Reynolds Averaged Navier-Stokes) simulation, which results in a LES (Large Eddy Simulation)-like behavior in unsteady regions of the flow field. At the same time, the model provides standard RANS capabilities in stable flow regions. More detailed descriptions of the SAS-SST model can be found in the ANSYS CFX-solver modeling guide [7].

Fig. 10 shows the grid system for the computational domain that had the same size as the test facility. A hybrid mesh, made up of tetrahedrons, wedges, pyramids and hexahedrons, was generated to prevent the oversimplification of the geometry, and to have more efficient mesh distribution. Prism layers were used to get higher resolution in the near-wall region. Total numbers of elements were 1.7×10^7 and maximum y+ was 24.

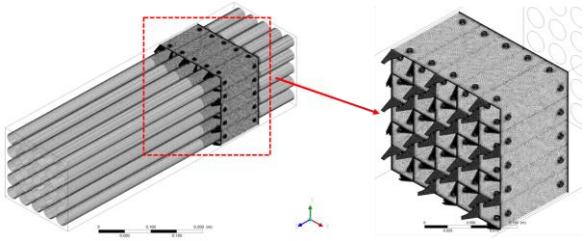

Fig. 10. Grid system.

Fully developed cross sectional profiles of velocity components, obtained from corresponding precursor simulation on Z-periodic thin rod bundle, were used as an inlet boundary condition. Turbulence intensity at the inlet was assumed to be 5 %. The 'average pressure over the whole outlet' option; with a relative pressure of 0 Pa, was used as an outlet-boundary condition. A no-slip condition was applied at the solid wall. To model the flow in the near-wall region, the automatic near wall treatment method was applied.

4.5 Results and Discussion

Fig. 11 ~ Fig. 13 shows the time averaged horizontal, vertical and axial velocity profile respectively at Y=0.5P and two different axial locations, Z=0.5D_h and 4.0D_h, from the downstream edge of the mixing vane tip.

The 1st order accurate upwind differencing (up-up) under-predicted peak velocity magnitude except the time averaged horizontal velocity at Z=4.0D_h and resulted in less variation in the velocity magnitude; compared with high resolution scheme (hi-hi). The reason is that the 1st order accurate upwind differencing may increase the numerical/false diffusion and may not provide the desired accuracy. Therefore it is recommended that the higher order accurate discretization scheme be used for a typical turbulent flow in the fuel assembly.

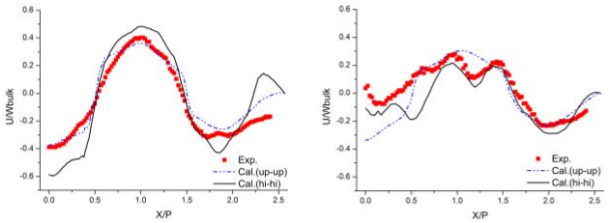

(a) Z=0.5D_h (b) Z=4.0D_h

Fig. 11. Time averaged horizontal velocity (U/W_{bulk}) profile at Y=0.5P

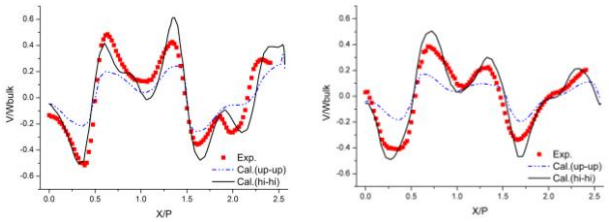

(a) Z=0.5D_h (b) Z=4.0D_h

Fig. 12. Time averaged vertical velocity (V/W_{bulk}) profile at Y=0.5P

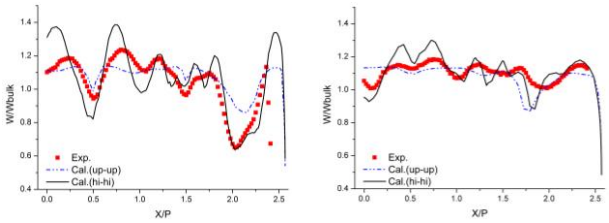

(a) Z=0.5D_h (b) Z=4.0D_h

Fig. 13. Time averaged axial velocity (W/W_{bulk}) profile at Y=0.5P

5. Conclusions

In this study, to examine the effect of the numerical order of accuracy of the discretization scheme on the prediction accuracy for the nuclear safety problems, simulations were conducted with the commercial CFD software, ANSYS CFX R.14 and FLUENT R.14. The predicted results were compared with the measured data for three test cases; (1) moderator test vessel, (2) 1/5 scaled-down APR+ model, (3) MATiS-H facility. Through these comparisons it was concluded that high order accurate schemes for the convection terms could not always guarantee the improved prediction for nuclear safety problems.

Whether mesh independent CFD solution can finally be obtained on the affordable mesh resolution is the most significant question to answer for reactor safety problems. If licensing applicants use CFD solution for their licensing documents, they should preferentially try

to demonstrate that the final result of the calculations is mesh independent. Additionally, if the above-mentioned requirement is not satisfied, they should conduct the sensitivity study for the numerical order of accuracy of the discretization scheme, and use the physically appropriate and conservative simulation results for their licensing documents

ACKNOWLEDGEMENT

This work was supported by the Nuclear Safety Research Program through the Korea Radiation Safety Foundation (KORSAFe) and the Nuclear Safety and Security Commission (NSSC), Republic of Korea (Grant No. 1305002). The authors gratefully thank Dr. Song, Dr. Jang and Dr. Lee in the KAERI for providing the MATiS-H experimental data and giving the valuable comments.

REFERENCES

[1] F. Menter, CFD Best Practice Guidelines for CFD Code Validation for Reactor Safety Applications, ECORA CONTRACT N° FIKS-CT-2001-00154, 2001.
[2] R. G. Huget, J. K. Szymanski, W. I. Midvidy, Experimental and Numerical Modelling of Combined Forced and Free Convection in a Complex Geometry with Internal Heat Generation, Proc. 9th Int. Heat Transfer Conf., 1990, Jerusalem, Israel.
[3] G. H. Lee, Y. S. Bang, A. J. Cheong, Comparative Study for Modeling Reactor Internal Geometry in CFD Simulation of PWR and PHWR Internal Flow, CFD4NRS-5, September 9-11, 2014, Zurich, Switzerland.
[4] ANSYS FLUENT User's Guide, ANSYS Inc., 2011.
[5] D. J. Euh, K. H. Kim, J. H. Youn, J. H. Bae, I. C. Chu, J. T. Kim, H. S. Kang, H. S. Choi, S. T. Lee, T. S. Kwon, A Flow and Pressure Distribution of APR+ Reactor under the 4-Pump Running Conditions with a Balanced Flow Rate, Nuclear Engineering and Technology, Vol.44, p.735, 2002.
[6] B. J. Lee, H. C. Jang, J. S. Cheong, S. J. Baek, Y. S. Park, A Review on the Regionalization Methodology for Core Inlet Flow Distribution Map, J. Korean Nuclear Society, Vol.33, p. 441, 2001.
[7] ANSYS CFX-Solver Modeling Guide, ANSYS Inc., 2011.
[8] G. H. Lee, Y. S. Bang, S. W. Woo, A. J. Cheong, Sensitivity Study on Turbulence Models for the Prediction of the Reactor Internal Flow, ICONE22-31255, Proceedings of the 22nd International Conference on Nuclear Engineering, July 7-11, 2014, Prague, Czech Republic.
[9] K. H. Kim, D. J. Euh, I. C. Chu, Y. J. Youn, H. S. Choi, T. S. Kwon, Experimental Study of the APR+ Reactor Core Flow and Pressure Distributions under 4-Pump Running Conditions, Nuclear Engineering and Design, Vol.265, p.957, 2013.
[10] S.-K. Chang, S. Kim, C.-H. Song, Turbulent Mixing in a Rod Bundle with Vaned Spacer Grids: OECD/NEA− KAERI CFD Benchmark Exercise Test, Nuclear Engineering and Design, DOI: 10.1016/j.nucengdes.2014.05.013, 2014.